Progress In Electromagnetics Research B, Vol. 32, 217–242, 2011

UNIFIED EFFICIENT FUNDAMENTAL ADI-FDTD SCHEMES FOR LOSSY MEDIA

D. Y. Heh* **and E. L. Tan**

School of Electrical and Electronic Engineering, Nanyang Technological University, 50, Nanyang Avenue, 639798, Singapore

Abstract—This paper presents the unified efficient fundamental alternating-direction-implicit finite-difference time-domain (ADI-FDTD) schemes for lossy media. The schemes presented include averaging, forward-forward, forward-backward and novel exponential time differencing schemes. Unifications of these schemes in both conventional and efficient fundamental forms of source-incorporated ADI-FDTD are provided. In the latter, they are formulated in the simplest, most concise, most efficient, and most fundamental form of ADI-FDTD. The unified update equations and implementation of the efficient fundamental ADI-FDTD schemes are provided. Such efficient fundamental schemes have substantially less right-hand-side update coefficients and field variables compared to the conventional ADI-FDTD schemes. Thus, they feature higher efficiency with reduced memory indexing and arithmetic operations. Other aspects such as field and parameter memory arrays, perfect electric conductor and perfect magnetic conductor implementations are also discussed. Numerical results in the realm of CPU time saving, asymmetry and numerical errors as well as specific absorption rate (SAR) of human skin are presented.

1. INTRODUCTION

The alternating-direction-implicit finite-difference time-domain (ADI-FDTD) method [1–3] has gained much prominence recently due to its unconditionally stable feature where the time step is no longer restricted by the Courant-Friedrich-Lewy (CFL) stability criterion. The popularity of ADI-FDTD method has further brought about the successful extensions into modeling lossy media [4–9], while retaining its unconditional stability feature. The proof of unconditional

Received 18 May 2011, Accepted 9 July 2011, Scheduled 18 July 2011

* Corresponding author: Ding Yu Heh (hehd0002@ntu.edu.sg).

stability feature for various ADI-FDTD schemes for lossy media has been provided in [10]. However, the conventional form of ADI-FDTD method has made the algorithm rather complicated. Apart from solving tridiagonal systems, the right-hand-sides (RHS) of the update equations involve many update coefficients and field variables (resultant from RHS matrix-operators) that require considerable arithmetic operations. Furthermore, one should not overlook the huge amount of memory indexing operations incurred throughout the whole procedures. The introduction of conductivity terms for lossy media into ADI-FDTD algorithm has made such overhead worse from the efficiency point of view where the arithmetic operations and memory indexing increase considerably. Furthermore, it is often desirable to formulate various schemes of ADI-FDTD method under unified schemes which feature higher efficiency and simplicity.

Recently, a new algorithm of efficient ADI-FDTD method [11] which features higher efficiency has been proposed. Such efficient ADI algorithm is included within a family of fundamental implicit schemes, which feature similar fundamental updating structures that are in simplest forms with most efficient matrix-operator-free RHS [12]. Extension of such efficient fundamental form of ADI-FDTD method for lossy media with forward-backward scheme has been discussed in [13], where the conductivity terms are applied at the forward time $(n+\frac{1}{2})$ in the first substep and backward time $(n+\frac{1}{2})$ in the second. In this paper, we consider many more schemes and further unify these schemes based on both conventional form (with RHS matrix-operators) and efficient fundamental form (with RHS matrix-operator-free) of ADI-FDTD for lossy media. Among the schemes considered are averaging, forward-forward, forward-backward and novel exponential time differencing (ETD) schemes (These schemes will be elaborated further in Section 2). The novel scheme based on the ETD [14, 15] is introduced for the first time (in the main grid) in efficient fundamental form of ADI-FDTD method, which also achieves higher accuracy compared to other schemes.

The organization of this paper is as follows. Section 2 presents various ADI-FDTD schemes for lossy media. Unifications of these schemes in both conventional and efficient fundamental forms of source-incorporated ADI-FDTD are then provided in Section 3. Subsequently, the detailed implementation of these unified efficient fundamental schemes for lossy media is provided in Section 4. Other aspects such as field and parameter memory arrays, perfect electric conductor (PEC) and perfect magnetic conductor (PMC) implementations are also discussed. In Section 5, numerical results which include CPU time saving (efficiency gain) as well as asymmetry and numerical errors

will be presented and discussed. The specific absorption rate (SAR) computation of human skin exposed to electromagnetic radiation will also be considered.

2. VARIOUS ADI-FDTD SCHEMES FOR LOSSY MEDIA

2.1. Averaging

The averaging scheme [4–6] is one of the most common schemes used where the conductivity terms are averaged between two time indices in both substeps. The scheme calls for the following update procedure:

$$\left(\mathbf{I} - \frac{\Delta t}{2}\mathbf{A} + \frac{\Delta t}{4}\mathbf{L}\right)\mathbf{u}^{n+\frac{1}{2}} = \left(\mathbf{I} + \frac{\Delta t}{2}\mathbf{B} - \frac{\Delta t}{4}\mathbf{L}\right)\mathbf{u}^{n} \tag{1a}$$

$$\left(\mathbf{I} - \frac{\Delta t}{2}\mathbf{B} + \frac{\Delta t}{4}\mathbf{L}\right)\mathbf{u}^{n+1} = \left(\mathbf{I} + \frac{\Delta t}{2}\mathbf{A} - \frac{\Delta t}{4}\mathbf{L}\right)\mathbf{u}^{n+\frac{1}{2}} \tag{1b}$$

where $\mathbf{I}$ is the 6×6 identity matrix, $\mathbf{A}$ and $\mathbf{B}$ are the splitting matrix operators commonly used in ADI-FDTD compact notations [12]:

$$\mathbf{A} = \begin{bmatrix} 0 & 0 & 0 & 0 & 0 & \frac{1}{\epsilon}\partial_y \\ 0 & 0 & 0 & \frac{1}{\epsilon}\partial_z & 0 & 0 \\ 0 & 0 & 0 & 0 & \frac{1}{\epsilon}\partial_x & 0 \\ 0 & \frac{1}{\mu}\partial_z & 0 & 0 & 0 & 0 \\ 0 & 0 & \frac{1}{\mu}\partial_x & 0 & 0 & 0 \\ \frac{1}{\mu}\partial_y & 0 & 0 & 0 & 0 & 0 \end{bmatrix} \tag{2}$$

$$\mathbf{B} = \begin{bmatrix} 0 & 0 & 0 & 0 & \frac{-1}{\epsilon}\partial_z & 0 \\ 0 & 0 & 0 & 0 & 0 & \frac{-1}{\epsilon}\partial_x \\ 0 & 0 & 0 & \frac{-1}{\epsilon}\partial_y & 0 & 0 \\ 0 & 0 & \frac{-1}{\mu}\partial_y & 0 & 0 & 0 \\ \frac{-1}{\mu}\partial_z & 0 & 0 & 0 & 0 & 0 \\ 0 & \frac{-1}{\mu}\partial_x & 0 & 0 & 0 & 0 \end{bmatrix} \tag{3}$$

and $\mathbf{L}$ is the diagonal loss matrix $\mathbf{L} = \mathrm{diag}([\frac{\sigma}{\epsilon}, \frac{\sigma}{\epsilon}, \frac{\sigma}{\epsilon}, \frac{\sigma^*}{\mu}, \frac{\sigma^*}{\mu}, \frac{\sigma^*}{\mu}])$. ∂_x, ∂_y and ∂_z are the spatial differential operator in x, y and z-directions, respectively. ϵ, μ, σ and σ^* are the medium permittivity, permeability, electric and magnetic conductivities, respectively. Note that the averaging scheme is second-order in temporal accuracy.

2.2. Forward-Forward

Another possible scheme is the forward-forward scheme [7], where the conductivity terms are applied at forward time for both substeps ($n+\frac{1}{2}$

for the first and $n+1$ for second). According to [7], such scheme allows effective modeling of highly conductive material. The scheme calls for the following update procedure:

$$\left(\mathbf{I} - \frac{\Delta t}{2}\mathbf{A} + \frac{\Delta t}{2}\mathbf{L}\right)\mathbf{u}^{n+\frac{1}{2}} = \left(\mathbf{I} + \frac{\Delta t}{2}\mathbf{B}\right)\mathbf{u}^{n} \tag{4a}$$

$$\left(\mathbf{I} - \frac{\Delta t}{2}\mathbf{B} + \frac{\Delta t}{2}\mathbf{L}\right)\mathbf{u}^{n+1} = \left(\mathbf{I} + \frac{\Delta t}{2}\mathbf{A}\right)\mathbf{u}^{n+\frac{1}{2}}. \tag{4b}$$

Note however that the forward-forward scheme is only first-order in temporal accuracy.

2.3. Forward-Backward

In forward-backward scheme [13], the conductivity terms are applied at the forward time $(n + \frac{1}{2})$ in the first substep and backward time $(n + \frac{1}{2})$ in the second. Such scheme allows exploitation of the efficient algorithm in [13] which feature programming simplicity, whereby the current density source and conductivity terms are added only to the first substep. The scheme calls for the following update procedure:

$$\left(\mathbf{I} - \frac{\Delta t}{2}\mathbf{A} + \frac{\Delta t}{2}\mathbf{L}\right)\mathbf{u}^{n+\frac{1}{2}} = \left(\mathbf{I} + \frac{\Delta t}{2}\mathbf{B}\right)\mathbf{u}^{n} \tag{5a}$$

$$\left(\mathbf{I} - \frac{\Delta t}{2}\mathbf{B}\right)\mathbf{u}^{n+1} = \left(\mathbf{I} + \frac{\Delta t}{2}\mathbf{A} - \frac{\Delta t}{2}\mathbf{L}\right)\mathbf{u}^{n+\frac{1}{2}}. \tag{5b}$$

The forward-backward scheme is second-order in temporal accuracy.

2.4. Exponential Time Differencing

It has been demonstrated in [16] that ETD scheme is generally better to model doubly lossy media in explicit FDTD method compared to other schemes. In this subsection, we incorporate the ETD scheme into ADI-FDTD method to reap its unconditionally stable advantage. The ETD scheme calls for the following update procedure:

$$(\mathbf{I} - \mathbf{CA})\,\mathbf{u}^{n+\frac{1}{2}} = \left(e^{-\mathbf{L}\frac{\Delta t}{2}} + \mathbf{CB}\right)\mathbf{u}^{n} \tag{6a}$$

$$(\mathbf{I} - \mathbf{CB})\,\mathbf{u}^{n+1} = \left(e^{-\mathbf{L}\frac{\Delta t}{2}} + \mathbf{CA}\right)\mathbf{u}^{n+\frac{1}{2}} \tag{6b}$$

where $\mathbf{C} = \mathbf{L}^{-1}(\mathbf{I} - e^{-\mathbf{L}\frac{\Delta t}{2}})$ is diagonal. Note that the ETD scheme is also second-order in temporal accuracy.

In addition to the schemes presented above, there are also other possible schemes including backward-forward and backward-backward

schemes. The former is essentially a dual of the forward-backward scheme, while the latter is found to be not unconditionally stable [10], and hence they shall not be discussed further in this paper.

3. UNIFICATIONS OF SOURCE-INCORPORATED ADI-FDTD SCHEMES FOR LOSSY MEDIA

3.1. Unified Conventional Form (with RHS Matrix-Operators)

The previous section has discussed many possible schemes in conventional form of ADI-FDTD method for lossy media, it would be desirable if all those schemes can be unified and generalized. The aforementioned schemes are first unified based on the conventional form of ADI-FDTD method as

$$(\mathbf{I} - \mathbf{A}_L)\,\mathbf{u}^{n+\frac{1}{2}} = (\mathbf{D}_u + \mathbf{B}_L)\,\mathbf{u}^n + \mathbf{D}_s\mathbf{s}^{n+\frac{1}{2}} \tag{7a}$$

$$(\mathbf{I} - \mathbf{B}_L)\,\mathbf{u}^{n+1} = (\mathbf{D}_u + \mathbf{A}_L)\,\mathbf{u}^{n+\frac{1}{2}} + \mathbf{D}_s\mathbf{s}^{n+\frac{1}{2}} \tag{7b}$$

Here, we have also incorporated the symmetric source implementation [17–19] where $\mathbf{s}$ is the current source vector. $\mathbf{D}_u$ (diagonal), $\mathbf{A}_L$, $\mathbf{D}_s$ (diagonal) and $\mathbf{B}_L$ for various schemes are listed in Table 1. With such formulation, all previous schemes can be concisely described by (7) along with Table 1. Such unified form is amenable to the same computer code for all the schemes, except possibly with different update coefficients. All schemes are directly reducible to the lossless case when $\mathbf{L}$ is null, except for ETD scheme where $\mathbf{A}_L$, $\mathbf{B}_L$ and $\mathbf{D}_s$ are undefined.

Table 1. Matrices for various ADI-FDTD schemes for lossy media.

Scheme	$\mathbf{A}_L$	$\mathbf{B}_L$
ETD	$\mathbf{L}^{-1}(\mathbf{I} - e^{-\mathbf{L}\frac{\Delta t}{2}})\mathbf{A}$	$\mathbf{L}^{-1}(\mathbf{I} - e^{-\mathbf{L}\frac{\Delta t}{2}})\mathbf{B}$
Avg	$\frac{\Delta t}{2}\left(\mathbf{I} + \frac{\Delta t}{4}\mathbf{L}\right)^{-1}\mathbf{A}$	$\frac{\Delta t}{2}\left(\mathbf{I} + \frac{\Delta t}{4}\mathbf{L}\right)^{-1}\mathbf{B}$
F-F	$\frac{\Delta t}{2}\left(\mathbf{I} + \frac{\Delta t}{2}\mathbf{L}\right)^{-1}\mathbf{A}$	$\frac{\Delta t}{2}\left(\mathbf{I} + \frac{\Delta t}{2}\mathbf{L}\right)^{-1}\mathbf{B}$
F-B	$\frac{\Delta t}{2}(\mathbf{A} - \mathbf{L})$	$\frac{\Delta t}{2}\mathbf{B}$
Scheme	$\mathbf{D}_u$	$\mathbf{D}_s$
ETD	$e^{-\mathbf{L}\frac{\Delta t}{2}}$	$\mathbf{L}^{-1}(\mathbf{I} - e^{-\mathbf{L}\frac{\Delta t}{2}})$
Avg	$\left(\mathbf{I} + \frac{\Delta t}{4}\mathbf{L}\right)^{-1}\left(\mathbf{I} - \frac{\Delta t}{4}\mathbf{L}\right)$	$\frac{\Delta t}{2}\left(\mathbf{I} + \frac{\Delta t}{4}\mathbf{L}\right)^{-1}$
F-F	$\left(\mathbf{I} + \frac{\Delta t}{2}\mathbf{L}\right)^{-1}$	$\frac{\Delta t}{2}\left(\mathbf{I} + \frac{\Delta t}{2}\mathbf{L}\right)^{-1}$
F-B	$\mathbf{I}$	$\frac{\Delta t}{2}$

ETD: Exponential Time Differencing; Avg: Averaging;
F-F: Forward-Forward; F-B: Forward-Backward

For ETD scheme, when $\mathbf{L}$ is approaching null, the expressions of $\mathbf{A}_L$, $\mathbf{B}_L$ and $\mathbf{D}_s$ can assume those of the averaging scheme because the update coefficients of the latter scheme is essentially a Pade approximation of the former scheme up to second order in time. Note however that (7) still involves matrix operators $\mathbf{A}$ and $\mathbf{B}$ (embedded in $\mathbf{A}_L$ and $\mathbf{B}_L$) at the RHS.

3.2. Unified Efficient Fundamental Form (with RHS Matrix-Operator-Free)

We next proceed to transform the unified schemes (7) into efficient fundamental form of ADI-FDTD method. Introducing the (temporary) auxiliary $\tilde{\mathbf{v}}$'s, (7) is rewritten as

$$\tilde{\mathbf{v}}^n = (\mathbf{D}_u + \mathbf{B}_L)\,\mathbf{u}^n \tag{8a}$$

$$(\mathbf{I} - \mathbf{A}_L)\,\mathbf{u}^{n+\frac{1}{2}} = \tilde{\mathbf{v}}^n + \mathbf{D}_s\mathbf{s}^{n+\frac{1}{2}} \tag{8b}$$

$$\tilde{\mathbf{v}}^{n+\frac{1}{2}} = (\mathbf{D}_u + \mathbf{A}_L)\,\mathbf{u}^{n+\frac{1}{2}} + \mathbf{D}_s\mathbf{s}^{n+\frac{1}{2}} \tag{8c}$$

$$(\mathbf{I} - \mathbf{B}_L)\,\mathbf{u}^{n+1} = \tilde{\mathbf{v}}^{n+\frac{1}{2}}. \tag{8d}$$

Next, (8d) is expressed at one time step backward as

$$\tilde{\mathbf{v}}^{n-\frac{1}{2}} = (\mathbf{I} - \mathbf{B}_L)\,\mathbf{u}^n \tag{9}$$

and (8a) can be subsequently reduced into

$$\begin{aligned}\tilde{\mathbf{v}}^n &= (\mathbf{D}_u + \mathbf{B}_L)\,\mathbf{u}^n = (\mathbf{I} + \mathbf{D}_u)\,\mathbf{u}^n - (\mathbf{I} - \mathbf{B}_L)\,\mathbf{u}^n \\ &= (\mathbf{I} + \mathbf{D}_u)\,\mathbf{u}^n - \tilde{\mathbf{v}}^{n-\frac{1}{2}}.\end{aligned} \tag{10}$$

Similarly, by rewriting (8b) as

$$\tilde{\mathbf{v}}^n = (\mathbf{I} - \mathbf{A}_L)\,\mathbf{u}^{n+\frac{1}{2}} - \mathbf{D}_s\mathbf{s}^{n+\frac{1}{2}}, \tag{11}$$

(8c) is reducible to

$$\begin{aligned}\tilde{\mathbf{v}}^{n+\frac{1}{2}} &= (\mathbf{D}_u + \mathbf{A}_L)\,\mathbf{u}^{n+\frac{1}{2}} + \mathbf{D}_s\mathbf{s}^{n+\frac{1}{2}} \\ &= (\mathbf{I} + \mathbf{D}_u)\,\mathbf{u}^{n+\frac{1}{2}} - \left[(\mathbf{I} - \mathbf{A}_L)\,\mathbf{u}^{n+\frac{1}{2}} - \mathbf{D}_s\mathbf{s}^{n+\frac{1}{2}}\right] \\ &= (\mathbf{I} + \mathbf{D}_u)\,\mathbf{u}^{n+\frac{1}{2}} - \tilde{\mathbf{v}}^n\end{aligned} \tag{12}$$

Finally, the unified schemes in efficient fundamental form of ADI-FDTD method read:

$$\tilde{\mathbf{v}}^n = (\mathbf{I} + \mathbf{D}_u)\,\mathbf{u}^n - \tilde{\mathbf{v}}^{n-\frac{1}{2}} \tag{13a}$$

$$(\mathbf{I} - \mathbf{A}_L)\,\mathbf{u}^{n+\frac{1}{2}} = \tilde{\mathbf{v}}^n + \mathbf{D}_s\mathbf{s}^{n+\frac{1}{2}} \tag{13b}$$

$$\tilde{\mathbf{v}}^{n+\frac{1}{2}} = (\mathbf{I} + \mathbf{D}_u)\,\mathbf{u}^{n+\frac{1}{2}} - \tilde{\mathbf{v}}^n \tag{13c}$$

$$(\mathbf{I} - \mathbf{B}_L)\,\mathbf{u}^{n+1} = \tilde{\mathbf{v}}^{n+\frac{1}{2}} \tag{13d}$$

with initialization $\tilde{\mathbf{v}}^{-\frac{1}{2}} = (\mathbf{I} - \mathbf{B}_L)\mathbf{u}^0$. Now, (13a), (13b) forms the first substep while (13c), (13d) forms the second. Note that (13) has been formulated in the simplest, most concise, most efficient, and most fundamental form of ADI-FDTD scheme with its RHS free of matrix operators **A** and **B** (It is the simplest because there are no more **A** and **B** to be simplified further at RHS). Besides, the source is incorporated concisely at only the first substep (13a), (13b) in the unified efficient fundamental ADI-FDTD schemes.

4. IMPLEMENTATION OF UNIFIED EFFICIENT FUNDAMENTAL ADI-FDTD SCHEMES

4.1. Unified Update Equations

We now provide the update equations for (13). Assuming only electric current density, J, and defining

$$\mathbf{u} = [E_x, E_y, E_z, H_x, H_y, H_z]^T \tag{14}$$

$$\tilde{\mathbf{v}} = [\tilde{e}_x, \tilde{e}_y, \tilde{e}_z, \tilde{h}_x, \tilde{h}_y, \tilde{h}_z]^T \tag{15}$$

$$\mathbf{s} = \left[\frac{-1}{\epsilon}J_x, \frac{-1}{\epsilon}J_y, \frac{-1}{\epsilon}J_z, 0, 0, 0,\right]^T, \tag{16}$$

the unified update equations of efficient fundamental ADI-FDTD schemes read
First substep from n to $n + \frac{1}{2}$

1) Auxiliary (explicit) update for $\tilde{e}_x^n$, $\tilde{h}_z^n$

$$\tilde{e}_x|^n_{i+\frac{1}{2},j,k} = c_{ea}E_x|^n_{i+\frac{1}{2},j,k} - \tilde{e}_x|^{n-\frac{1}{2}}_{i+\frac{1}{2},j,k} \tag{17a}$$

$$\tilde{h}_z|^n_{i+\frac{1}{2},j+\frac{1}{2},k} = c_{ha}H_z|^n_{i+\frac{1}{2},j+\frac{1}{2},k} - \tilde{h}_z|^{n-\frac{1}{2}}_{i+\frac{1}{2},j+\frac{1}{2},k} \tag{17b}$$

2) Implicit update for $E_x^{n+\frac{1}{2}}$

$$\left(1+\frac{bd}{\Delta y^2}+\frac{bd_-}{\Delta y^2}\right)E_x|^{n+\frac{1}{2}}_{i+\frac{1}{2},j,k} - \frac{bd}{\Delta y^2}E_x|^{n+\frac{1}{2}}_{i+\frac{1}{2},j+1,k} - \frac{bd_-}{\Delta y^2}E_x|^{n+\frac{1}{2}}_{i+\frac{1}{2},j-1,k}$$
$$= c_{e1}\tilde{e}_x|^n_{i+\frac{1}{2},j,k} + \frac{c_{e2}}{\Delta y}\tilde{h}_z|^n_{i+\frac{1}{2},j+\frac{1}{2},k} - \frac{c_{e3}}{\Delta y}\tilde{h}_z|^n_{i+\frac{1}{2},j-\frac{1}{2},k} - c_{e4}J_x|^{n+\frac{1}{2}}_{i+\frac{1}{2},j,k} \tag{18}$$

3) Explicit update for $H_z^{n+\frac{1}{2}}$

$$H_z|^{n+\frac{1}{2}}_{i+\frac{1}{2},j+\frac{1}{2},k} = c_{h1}\tilde{h}_z|^n_{i+\frac{1}{2},j+\frac{1}{2},k} + \frac{c_{h2}}{\Delta y}\left(E_x|^n_{i+\frac{1}{2},j+1,k} - E_x|^n_{i+\frac{1}{2},j,k}\right). \tag{19}$$

Table 2. Coefficients and parameters of update equations for various efficient fundamental ADI-FDTD schemes.

Scheme	Implicit Update				Explicit Update			
	c_{e1}	c_{e2}	c_{e3}	c_{e4}	c_{h1}	c_{h2}	c_{ea}	c_{ha}
ETD	1	b	b	b	1	d	$1+p$	$1+q$
Avg	1	b	b	b	1	d	p	q
F-F	1	b	b	b	1	d	$1+p$	$1+q$
F-B	p	bq	bq_-	b	$2q$	d	2	2

Scheme	b	d	p	q
ETD	$\frac{1-e^{-\Delta t\sigma/2\epsilon}}{\sigma}$	$\frac{1-e^{-\Delta t\sigma^*/2\mu}}{\sigma^*}$	$e^{-\Delta t\sigma/2\epsilon}$	$e^{-\Delta t\sigma^*/2\mu}$
Avg	$\frac{\Delta t/2\epsilon}{\left(1+\frac{\Delta t\sigma}{4\epsilon}\right)}$	$\frac{\Delta t/2\mu}{\left(1+\frac{\Delta t\sigma^*}{4\mu}\right)}$	$\frac{2}{\left(1+\frac{\Delta t\sigma}{4\epsilon}\right)}$	$\frac{2}{\left(1+\frac{\Delta t\sigma^*}{4\mu}\right)}$
F-F	$\frac{\Delta t/2\epsilon}{\left(1+\frac{\Delta t\sigma}{2\epsilon}\right)}$	$\frac{\Delta t/2\mu}{\left(1+\frac{\Delta t\sigma^*}{2\mu}\right)}$	$\frac{1}{\left(1+\frac{\Delta t\sigma}{2\epsilon}\right)}$	$\frac{1}{\left(1+\frac{\Delta t\sigma^*}{2\mu}\right)}$
F-B	$\frac{\Delta t/2\epsilon}{\left(1+\frac{\Delta t\sigma}{2\epsilon}\right)}$	$\frac{\Delta t/2\mu}{\left(1+\frac{\Delta t\sigma^*}{2\mu}\right)}$	$\frac{1}{\left(1+\frac{\Delta t\sigma}{2\epsilon}\right)}$	$\frac{1}{\left(1+\frac{\Delta t\sigma^*}{2\mu}\right)}$

All the update coefficients and associated parameters for various schemes are tabulated in Table 2. Note that for simplicity, we have omitted the subscript indices for all media parameters ϵ, σ, μ, σ^* and b, d, p, q. In fact, the subscript indices of ϵ, σ, b and p should follow that of the electric fields, whereas those of μ, σ^*, d and q follow that of the magnetic fields. For instance, in the above update equations, cf. (17)–(19), b and p have subscript indices of $i+\frac{1}{2}, j, k$ while d and q have those of $i+\frac{1}{2}, j+\frac{1}{2}, k$. For d_- and q_-, the subscript indices are $i+\frac{1}{2}, j-\frac{1}{2}, k$ where $d_- = d_{i+\frac{1}{2},j-\frac{1}{2},k}$ and $q_- = q_{i+\frac{1}{2},j-\frac{1}{2},k}$.

The update equations for all other field components can be written down by permuting the subscript indices of the parameters, fields and spatial steps. Similar procedures can then be performed to derive the update equations for the second substep. It should be reminded that no electric current source J is needed in the second substep, which is made possible by the efficient fundamental form (13c), (13d). For forward-backward scheme, note also that the update coefficients in the second substep are derived by setting σ and σ^* equal zero (lossless) [13].

Examining (18) indicates that the number of RHS update coefficients and field variables are substantially lower than that of the conventional ADI-FDTD schemes (Eq. (11) in [4]). Moreover, a look at Table 2 reveals that the update coefficients c_{e2}, c_{e3} and c_{e4} are the same (independent of μ and σ^*) for ETD, averaging and forward-forward schemes. This is particularly useful for inhomogeneous magnetic media where no additional memory indexing is required in the electric

Table 3. Comparisons of number of arithmetic operations per grid between conventional and efficient fundamental forms of ADI-FDTD schemes for lossy media over one complete time step.

Arithmetic operations		Conventional form	Efficient fundamental form
Implicit, RHS	M/D	84	12
	A/S	48	12
Explicit, RHS	M/D	30	30
	A/S	24	24
Total, RHS	M/D	114	42
	A/S	72	36
	M/D + A/S	186	78
Tridiag. matrices inversion	M/D	18	18
	A/S	12	12
Overall	M/D	132	60
	A/S	84	48
	M/D + A/S	216	108
Efficiency gain	RHS	1	2.38
	Overall	1	2

field update Equations (18). For forward-backward scheme, the simplicity lies in the second substep where the algorithm is as easy as implementing a lossless ADI-FDTD method. Lastly, the symmetric current source excitation [17–19] is only needed in the first substep for all efficient fundamental schemes. All the aforementioned advantages contribute towards reducing the flops count and memory indexing throughout the whole update procedures and thus improving the overall efficiency compared to the conventional ADI-FDTD schemes.

Table 3 shows the comparisons of number of arithmetic operations per grid between conventional and efficient fundamental forms of ADI-FDTD schemes for lossy media over one complete time step. The number of multiplications/divisions (M/D) and additions/subtractions (A/S) are determined from (7a), (7b) for conventional form of ADI-FDTD and (13a)–(13d) for efficient fundamental form of ADI-FDTD. We can see that the total flops count for the RHS is considerably less for the efficient fundamental form (78 against 186 for conventional form), which gives an efficiency gain of 2.38. Since there is cost for solving tridiagonal systems, Table 3 also includes the arithmetic operations needed for inverting tridiagonal matrices. The algorithm used for the tridiagonal matrices inversion is Thomas algorithm, which is a special

type of Gaussian elimination method. Taking this cost into account, the efficient fundamental form still achieves an overall efficiency gain of 2.

4.2. Field Memory Arrays

The field memory arrays needed for efficient fundamental ADI-FDTD schemes are initially found to be ($\xi = x, y, z$)

$$\begin{aligned} &\left\{\tilde{e}_\xi^{n-\frac{1}{2}}, \tilde{e}_\xi^{n}, \tilde{e}_\xi^{n+\frac{1}{2}}\right\}; \quad \left\{E_\xi^{n}, E_\xi^{n+\frac{1}{2}}, E_\xi^{n+1}\right\}; \\ &\left\{\tilde{h}_\xi^{n-\frac{1}{2}}, \tilde{h}_\xi^{n}, \tilde{h}_\xi^{n+\frac{1}{2}}\right\}; \quad \left\{H_\xi^{n}, H_\xi^{n+\frac{1}{2}}, H_\xi^{n+1}\right\} \end{aligned} \tag{20}$$

where the variables grouped within the same curly braces share the same memory arrays, i.e., in computer programs, they share the same variable names to be assigned with new values successively. For instance, $\{\tilde{e}_\xi^{n-\frac{1}{2}}, \tilde{e}_\xi^{n}, \tilde{e}_\xi^{n+\frac{1}{2}}\}$ consume 1 field memory array and the same holds for $\{E_\xi^{n}, E_\xi^{n+\frac{1}{2}}, E_\xi^{n+1}\}$, $\{\tilde{h}_\xi^{n-\frac{1}{2}}, \tilde{h}_\xi^{n}, \tilde{h}_\xi^{n+\frac{1}{2}}\}$ and $\{H_\xi^{n}, H_\xi^{n+\frac{1}{2}}, H_\xi^{n+1}\}$. Since there are x, y and z-directed fields ($\xi = x, y, z$), the total number of field memory arrays needed are $4 \times 3 = 12$.

To reduce the field memory storage, one can combine (19) with (17b) in the next half time step $(n + \frac{1}{2})$ to yield

$$\begin{aligned} &\tilde{h}_z\big|_{i+\frac{1}{2},j+\frac{1}{2},k}^{n+\frac{1}{2}} \\ &= (c_{ha}c_{h1}-1)\tilde{h}_z\big|_{i+\frac{1}{2},j+\frac{1}{2},k}^{n} + \frac{c_{ha}c_{h2}}{\Delta y}\left(E_x\big|_{i+\frac{1}{2},j+1,k}^{n+\frac{1}{2}} - E_x\big|_{i+\frac{1}{2},j,k}^{n+\frac{1}{2}}\right). \end{aligned} \tag{21}$$

This can always be done because we are not interested in the intermediate magnetic field values at $n + \frac{1}{2}$. In this case, the explicit update of (19) is no longer needed and the efficiency can be further improved. Furthermore, if the final magnetic field values are not frequently needed, we can repeat the above procedures for the final magnetic field update equations in the second substep. In doing so, the field memory arrays needed are now

$$\left\{\tilde{e}_\xi^{n-\frac{1}{2}}, \tilde{e}_\xi^{n}, \tilde{e}_\xi^{n+\frac{1}{2}}\right\}; \quad \left\{E_\xi^{n}, E_\xi^{n+\frac{1}{2}}, E_\xi^{n+1}\right\}; \quad \left\{\tilde{h}_\xi^{n-\frac{1}{2}}, \tilde{h}_\xi^{n}, \tilde{h}_\xi^{n+\frac{1}{2}}\right\}. \tag{22}$$

Now the total number of field memory arrays needed is $3 \times 3 = 9$.

For comparison, we note that in conventional ADI-FDTD schemes, the field memory arrays are given as

$$\left\{E_\xi^{n}, E_\xi^{n+1}\right\}; \quad \left\{E_\xi^{n+\frac{1}{2}}\right\}; \quad \left\{H_\xi^{n}, H_\xi^{n+\frac{1}{2}}, H_\xi^{n+1}\right\}. \tag{23}$$

The total number of field memory arrays needed is also $3 \times 3 = 9$, which is the same as the efficient fundamental ADI-FDTD schemes.

4.3. Parameter Memory Arrays

Conventionally, all coefficients in Table 2 are computed in run time during each iteration from four media parameter memory arrays, which comprise

$$\{\epsilon\}; \quad \{\mu\}; \quad \{\sigma\}; \quad \{\sigma^*\}. \tag{24}$$

To further improve the efficiency, instead of storing (24), we can first precompute and store the following four alternative parameter memory arrays:

$$\{b\}; \quad \{d\}; \quad \{p\}; \quad \{q\}. \tag{25}$$

It can be seen from Table 2 that, with the above alternative parameter memory arrays, all the respective RHS coefficients can be directly computed. This not only reduces the memory indexing effort but also reduces the arithmetic operations needed. For instance, with the alternative parameter memory arrays, to compute c_{e2} for ETD, averaging and forward-forward schemes, one would only need to access b instead of both ϵ and σ. No further arithmetic operations are needed. Note that such redefinition and storing of alternative parameter memory arrays is not effectively applicable in forward-backward scheme. This is because unlike the other schemes, the update coefficients of forward-backward scheme are different in both substeps (lossless in second substep).

4.4. PEC and PMC Implementations

Recently, PEC condition implementation within a computation domain for ADI-FDTD method has been considered in [20] by means of a modified tridiagonal matrix. Although it provides sufficient accuracy, the implementation is rather cumbersome, especially when the intended PEC structure is of arbitrary shape and not planar in nature. In this subsection, we make use of our efficient fundamental ADI-FDTD schemes for lossy media to implement PEC or PMC conveniently inside a computation domain. This can be directly realized by taking the limit of all the update coefficients tabulated in Table 2 when σ or σ^* tends to infinity. Note that such limit exists for all efficient fundamental ADI-FDTD schemes. Although the update procedures of the conventional ADI-FDTD schemes are not shown explicitly, it should be pointed out that for its forward-backward scheme, some RHS update coefficients of second substep will be undefined when σ or σ^* tends to infinity. Therefore, the

implementation of PEC or PMC will fail in the forward-backward scheme in conventional form of ADI-FDTD method, but not in the forward-backward scheme in our efficient fundamental form of ADI-FDTD method.

5. NUMERICAL RESULTS

5.1. CPU Time Saving

In this subsection, we compute the CPU time needed to run using various schemes of ADI-FDTD for lossy media in a PEC cavity of $50 \times 50 \times 51$ cells. The programs have been compiled using Microsoft Visual C++ under Microsoft Windows XP operating system (OS), and run on a platform of 2.66 GHz Intel Duo Core Processor with 4 GB RAM. We consider the alternative parameter memory arrays given in (25), i.e., all the respective RHS coefficients are directly computed, to reduce all the memory indexing effort and arithmetic operations. ϵ, μ, σ and σ^* can be of arbitrary values at different grid points. Cell size is set at 50 mm and Δt is specified at CFLN = 5 where CFLN = $\Delta t/\Delta t_{CFL}$, and Δt_{CFL} is the CFL limit in Yee's explicit FDTD method. A z-directed monochromatic sinusoidal point current source with frequency 300 MHz is excited at the centre (i_s, j_s, k_s) of the cavity. The program is run for a total of 100 time steps.

Table 4 shows the relative CPU time incurred for various ADI-FDTD schemes for lossy media, with respect to the reference Yee's explicit FDTD method [1]. The forward-backward scheme is omitted because the storing of alternative parameter memory arrays of (25) is not effectively applicable as mentioned earlier. Note that the time step used in the reference Yee's explicit FDTD method is set at its maximum allowed limit of CFLN = 1 to ensure stability. All ADI-FDTD schemes incurs the same relative CPU time due to the fact that all RHS coefficients are precomputed. At CFLN = 5, the conventional form of ADI-FDTD schemes incur relative CPU time of 0.83 while the efficient fundamental form of ADI-FDTD schemes incur relative CPU time of 0.33. With the aforementioned advantages of the efficient fundamental form of ADI-FDTD schemes (such as reduced RHS coefficients, field variables, etc.), the efficiency gain over the conventional form of ADI-FDTD schemes is around 2.5. Moreover, if compared against the Yee's explicit FDTD method, the efficiency gain is further increased to 3. This makes our efficient fundamental form of ADI-FDTD schemes attractive for its high algorithm efficiency. The RAM needed for efficient fundamental form of ADI-FDTD schemes is the same as the conventional form counterpart but higher than the Yee's explicit FDTD due to additional field memory arrays.

Table 4. Relative CPU time for various ADI-FDTD schemes for lossy media.

ADI-FDTD	Relative CPU time		
	Avg	ETD	F-F
Conventional form	0.83	0.83	0.83
Efficient fundamental form	0.33	0.33	0.33
Efficiency gain over conventional ADI-FDTD	2.5	2.5	2.5
Efficiency gain over explicit FDTD	3.0	3.0	3.0

Table 5. Efficiency gain in terms of CPU time achieved by efficient fundamental form over conventional form of ADI-FDTD and explicit FDTD for different computational domain sizes.

Domain size	Efficiency gain over	
	conventional ADI-FDTD	explicit FDTD
$50 \times 50 \times 50$	2.5	3.0
$100 \times 100 \times 100$	2.1	3.0
$250 \times 250 \times 250$	1.3	2.0

Table 5 further shows the efficiency gain in terms of CPU time achieved by efficient fundamental form over conventional form of ADI-FDTD and explicit FDTD for different computational domain sizes. For $50 \times 50 \times 50$ and $100 \times 100 \times 100$ computational domain sizes, the efficiency gain over the conventional form of ADI-FDTD is around 2 to 2.5 while the efficiency gain over the explicit FDTD is 3. For large computational domain size of $250 \times 250 \times 250$, the efficient fundamental form of ADI-FDTD still achieves an efficiency gain of 1.3 and 2 over conventional ADI-FDTD and explicit FDTD, respectively. The lower efficiency gain in large computational domain size may be attributed to the bottleneck caused by the memory indexing, where its computational cost is more expensive than the computational cost of arithmetic operations.

5.2. Numerical Examples for PEC and PMC Implementations

The implementation of PEC and PMC can also be used as a gauge for accuracy assessment for the efficient fundamental ADI-FDTD schemes detailed. For this purpose, we consider a $50 \times 50 \times 50$ cells cavity of uniform cell size 3 mm with a PEC sphere located at the centre and the rest free space. The radius of the PEC sphere is 30 mm. The

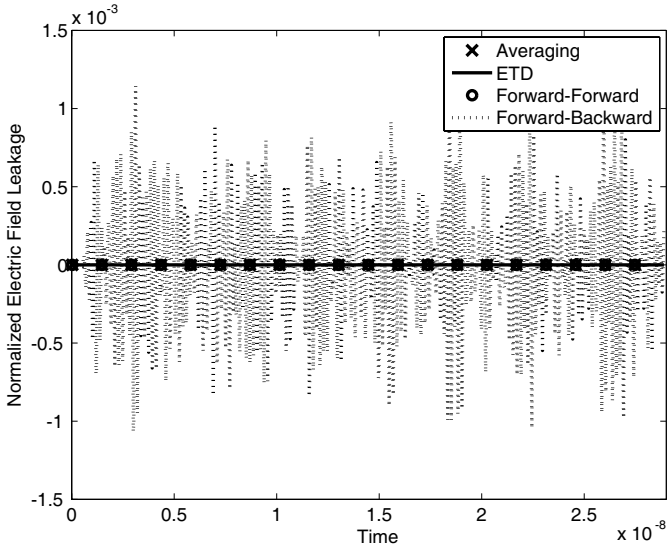

Figure 1. Normalized electric field leakage recorded at the centre of PEC sphere using different schemes. Only forward-backward scheme exhibits electric field leakage.

PEC medium is realized by setting σ to the extreme value of 10^{308}. A z-directed line current source of modulated Gaussian pulse with centre frequency 5 GHz extending from top to bottom of the cavity is located 24 mm away from the PEC sphere. The source illuminates upon the PEC sphere and the electric field leakage is measured at the centre of the PEC sphere throughout 1000 time steps with CFLN equals 5. The numerical experiments are carried out using different efficient fundamental ADI-FDTD schemes detailed. The PEC sphere is then replaced by a PMC sphere by setting σ^* to 10^{308} instead of σ, and the electric field leakage is also measured at the centre of the PMC sphere.

Figures 1 and 2 show the electric field leakage recorded at centre of PEC and PMC spheres normalized to the maximum value of electric field at the exterior. Analytically, no fields shall be able to penetrate the PEC or PMC material. We note that all three averaging, ETD and forward-forward schemes record zero electric field at the centre of the PEC and PMC spheres. On the contrary, forward-backward scheme records a field leakage of around 0.1 percent, which indicates the inaccuracy of the scheme.

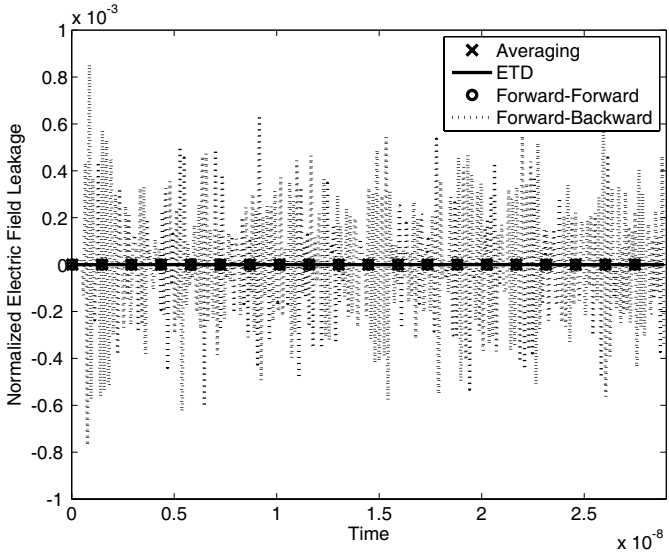

Figure 2. Same as Fig. 1, but for PMC sphere. Again, only forward-backward scheme exhibits electric field leakage.

5.3. Asymmetry and Numerical Errors

Next, we proceed to analyze the asymmetry and numerical errors posed by various ADI-FDTD schemes for lossy media. Comparisons of these errors could be made with either conventional or efficient fundamental form since both forms can be transformed into each other (and essentially yield the same computation). We adopt a dimension of $20 \times 20 \times 21$ cells, $\epsilon = \epsilon_0$, $\mu = \mu_0$, $\sigma = 10^{-4}\,\mathrm{S/m}$ and $\sigma^* = 0.05\,\Omega/\mathrm{m}$. Cell size, Δt and source are the same as the previous subsection. We also define the electric field asymmetry error as

$$E_{asymerr} = 20 \log \frac{|E_{z(i,j,ks)} - E_{z(j,i,ks)}|}{\max(|E_z|)} \tag{26}$$

Figure 3 shows the asymmetry error (in dB) with respect to x and y grid positions for various ADI-FDTD schemes. It can be seen that averaging, ETD and forward-forward schemes have very low level of electric field asymmetry error (in the vicinity of $-320\,\mathrm{dB}$). On the other hand, even though symmetric source is implemented, forward-backward scheme still records considerably higher electric field asymmetry error. We hereby point out that the symmetric source implementation described in [17–19] also utilized forward-backward scheme for its independent current source J, i.e., J is forward (at

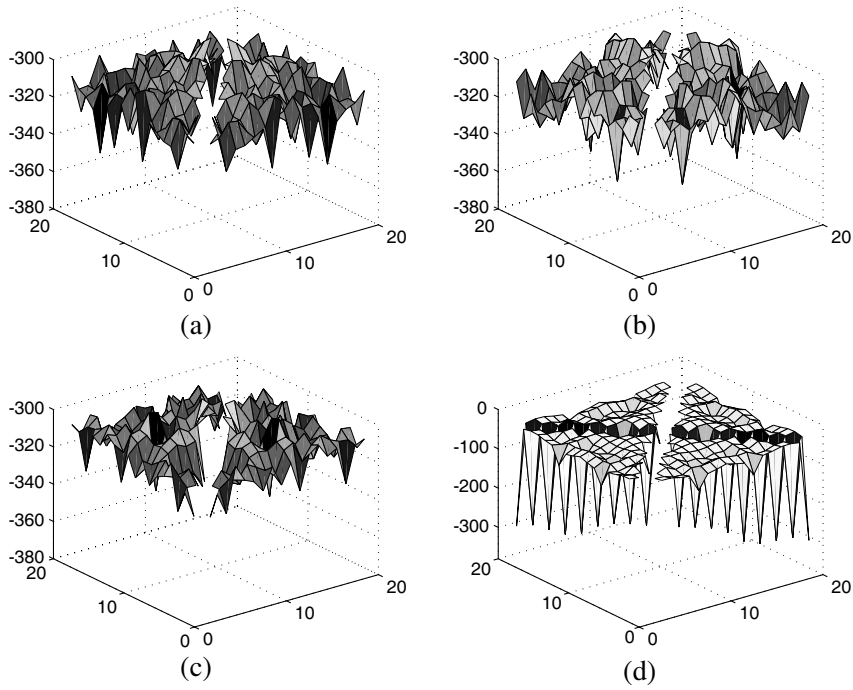

Figure 3. Asymmetry error (in dB) with respect to x and y grid positions for (a) exponential time differencing, (b) averaging, (c) forward-forward and (d) forward-backward schemes. Forward-backward scheme records considerably higher electric field asymmetry error.

$n + \frac{1}{2}$) in the first substep and backward (still at $n + \frac{1}{2}$) in the second. While it was shown previously that the forward-backward scheme of an *independent* source is accurate and has lower electric field asymmetry error, similar argument cannot be applied here if the source is *dependent* on electric field, such as in the case of lossy media here, where $J = \sigma E$.

To further compare the accuracy among ETD, averaging and forward-forward schemes, we now consider $20 \times 20 \times 21$ cells cavity of doubly lossy media with $\sigma = 0.3\,\mathrm{S/m}$ and $\sigma^* = 60\,\Omega/\mathrm{m}$. A z-directed line current source with modulated gaussian pulse excitation of centre frequency 300 MHz and bandwidth 600 MHz is flowing from bottom to top through the cavity centre. Cell size is now chosen as 16 mm to resolve 1/20 times of the medium wavelength. Simulation is terminated after 200 and 100 time steps with CFLN equals 5 and 10,

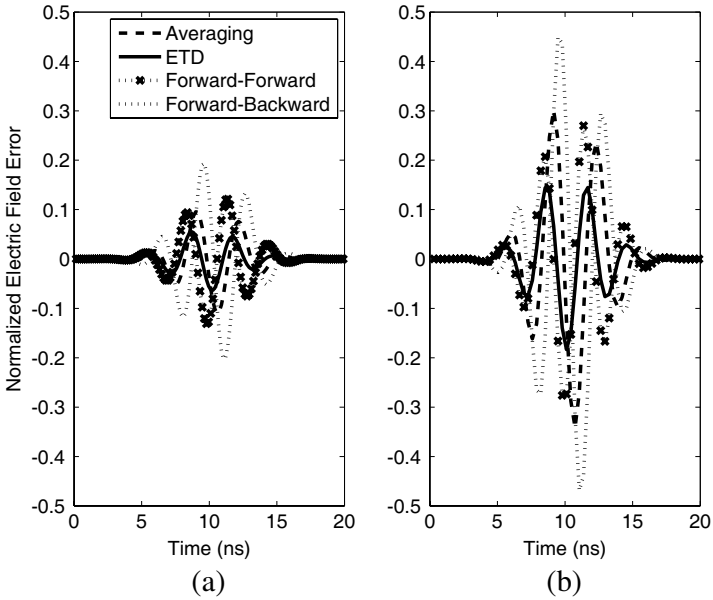

Figure 4. Normalized electric field error exhibited by various schemes for (a) CFLN = 5 and (b) CFLN = 10.

respectively. The experiment is also run using explicit FDTD method of time-averaging scheme [1], with Δt set at the CFL limit to serve as the reference. We define the normalized electric field error as

$$E_{err} = \frac{E_{ADI} - E_{explicit}}{\max(|E_{explicit}|)} \tag{27}$$

where E_{ADI} is the electric field recorded by various efficient fundamental form of ADI-FDTD schemes and $E_{explicit}$ is the electric field recorded by the explicit FDTD method. Fig. 4 shows the normalized electric field error recorded at position (17,17,17) using various schemes at (a) CFLN = 5 and (b) CFLN = 10, respectively. The normalized error shown by ETD scheme is the lowest among all, followed by averaging, forward-forward and lastly forward-backward schemes. Note that although forward-forward scheme is only first-order accurate in time, the overall accuracy is higher than that of forward-backward scheme, which may be due to the higher asymmetry error exhibited by the latter. The highest accuracy of ETD scheme may be attributed to its closer resemblance of solution to the first-order differential equation.

Table 6 further shows the efficiency gain and relative root-mean-square (RMS) error of efficient fundamental ADI-FDTD schemes for

Table 6. Efficiency gain and relative root-mean-square error of efficient fundamental ADI-FDTD schemes for various CFLNs.

CFLN		2	4	6	8	10
Efficiency gain		1.2	2.4	3.6	4.8	6.0
Relative RMS error	ETD	1.57%	4.38%	6.84%	8.96%	11.02%
	Avg	1.95%	6.32%	11.44%	16.18%	19.84%
	F-F	2.56%	4.83%	7.38%	10.08%	12.93%

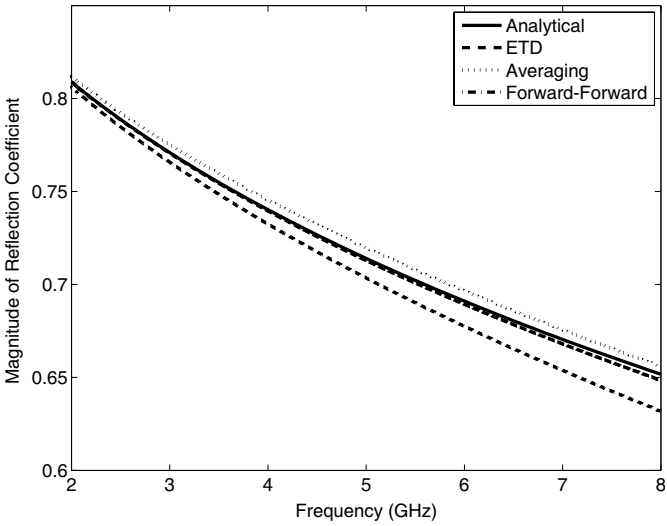

Figure 5. Magnitude of reflection coefficient for a half space lossy medium computed using various schemes.

various CFLNs. The efficiency gain is taken over the explicit FDTD and the RMS error is taken relative to the explicit FDTD within the whole computational domain for a sinusoidal excitation of 300 MHz. Cell per wavelength (CPW) is set as 20 which corresponds to cell size of 16 mm. This table gives a clear illustration on the trade-off between accuracy and efficiency of our efficient fundamental ADI-FDTD schemes. For practical CFLN of 4, the efficiency gain is 2.4, and the relative RMS error of all schemes ranges only from 4–6 percent. Even at CFLN = 10, our ETD scheme consumes 6 times less simulation time than the explicit FDTD, at the expense of only 11 percent relative RMS error. This implies that our efficient fundamental form of ADI-FDTD schemes achieves a good trade-off between efficiency and accuracy.

Table 7. Relative permittivity, ϵ_r and conductivity, σ of skin layers at 42.25 GHz and 61.22 GHz.

Skin layers	ϵ_r		σ	
	42.25 GHz	61.22 GHz	42.25 GHz	61.22 GHz
epidermis and dermis	11.40	8.00	33.00	37.40
fat	3.37	3.12	2.28	2.83

Finally, we compute the reflection coefficients of a half space lossy medium numerically. σ and σ^* of the lossy medium is set as 5 S/m and 60 Ω/m respectively. A modulated Gaussian pulse with a bandwidth of 6 GHz around centre frequency of 5 GHz is launched from the free space. Cell size is set at 0.9375 mm which corresponds to CPW of around 20 for the lossy medium at 5 GHz and CFLN = 4. The reflection coefficients in frequency domain can be obtained numerically by taking the ratio of the discrete Fourier transform of the reflected wave to the discrete Fourier transform of the incident wave. Fig. 5 plots the magnitude of reflection coefficient for a half space lossy medium computed using various schemes and they are compared against the reference analytical reflections coefficient Γ given as

$$\Gamma = \frac{\eta_2 - \eta_1}{\eta_1 + \eta_2} \tag{28}$$

where η_1 is the wave impedance of free space at 377 Ω and η_2 is the wave impedance of the lossy medium. It is evident that the magnitude of reflection coefficient computed using ETD scheme is the closest to the magnitude of reference analytical reflection coefficient. This again shows the highest accuracy of ETD scheme among all other schemes.

5.4. Specific Absorption Rate (SAR)

The specific absorption rate (SAR) is a measure of energy absorption rate for biological media exposed to electromagnetic radiation. It can be computed from

$$SAR = \frac{1}{2}\frac{\sigma|\tilde{\mathbf{E}}|^2}{\rho} \tag{29}$$

where $\tilde{\mathbf{E}}$ is the Fourier transform of the recorded electric field components and ρ is the density of the biological media in kg/m^3. The SAR has the overall unit of W/kg.

In this numerical example, the exposure of human skin to electromagnetic radiation is considered. The human skin has a cross sectional area of 3.75 mm $\times$3.75 mm in y and z directions and a depth

of 2 mm in x direction. In x direction, the skin has two layers. The top layer consists of epidermis and dermis which has a total thickness of 1.5 mm, and the bottom layer consists of fat. The interaction of human skin with electromagnetic waves at two therapeutic frequencies of 42.25 GHz and 61.22 GHz are considered [21]. The relative permittivity, ϵ_r and conductivity, σ of the skin layers at these two frequencies are listed in Table 7 [22]. The cell size $\Delta x = \Delta y = \Delta z = \Delta$ is chosen at 75 µm and a z-directed line current source located 1.5 mm away from the surface of the human skin illuminates upon it. The computational domain size is $50 \times 50 \times 50$ and 10 layers of perfectly matched layer (PML) [23–26] terminates the computational boundaries. The exterior boundaries of the PML is simply terminated with PEC. The perfectly matched layer used is the complex frequency shifted convolutional perfectly matched layer (CFS-CPML) having constitutive parameters

$$\sigma(\zeta) = \frac{\sigma_{\max} \mid \zeta - \zeta_0 \mid^m}{\delta^m} \tag{30}$$

$$\kappa(\zeta) = 1 + (\kappa_{\max} - 1)\frac{\mid \zeta - \zeta_0 \mid^m}{\delta^m} \tag{31}$$

where δ is the thickness of the PML, ζ_0 is the interface to free space and m is the order of the polynomial. In our simulation, $m = 4$, $\kappa_{\max} = 15$ and another constitutive parameter, α is set as a constant 0.08. $\sigma_{\max}$ that will minimize reflection is given as

$$\sigma_{\max} = \frac{m+1}{150\pi\Delta} = 141.49\,\mathrm{S/m}. \tag{32}$$

The SAR of human skin at 42.25 GHz and 61.22 GHz is computed using (29) at steady state. The densities of the top layer (epidermis and dermis) and bottom layer (fat) are assumed as $1000\,\mathrm{kg/m^3}$ and $850\,\mathrm{kg/m^3}$, respectively. Figs. 6 and 7 plot the SAR of human skin at 42.25 GHz and 61.22 GHz, respectively. Both figures show the SAR at z cut plane of 2 mm. The SAR values at each location have been scaled to correspond to incident power density $S = \frac{1}{2}\,\mathrm{Re}(\tilde{\mathbf{E}} \times \tilde{\mathbf{H}}^*)$ of $1\,\mathrm{mW/m^2}$ in free space. The SAR is computed using the efficient fundamental form of ADI-FDTD method with ETD scheme at CFLN = 5. It can be seen that at 61.22 GHz, the maximum SAR at the surface of the human skin is higher than that of 42.25 GHz and the SAR quickly decreases with respect to the depth (x axis) of human skin. Fig. 8 further plots the SAR of human skin at $y = 2$ mm with respect to only the depth. It is observed that the SAR at 61.22 GHz decreases at a higher rate along the depth of human skin compared to the SAR at 42.25 GHz. At depth of less than 0.3 mm, the human skin experiences more absorption at 61.22 GHz. Beyond 0.3 mm, the absorption at 42.25 GHz is more.

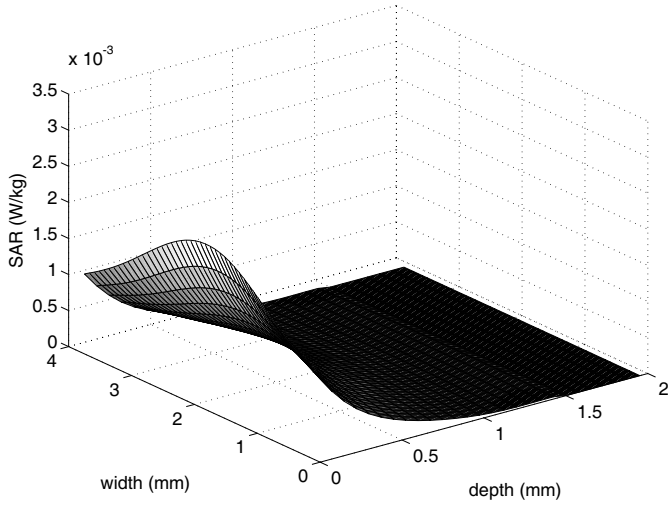

Figure 6. SAR of human skin at 42.25 GHz with respect to depth and width.

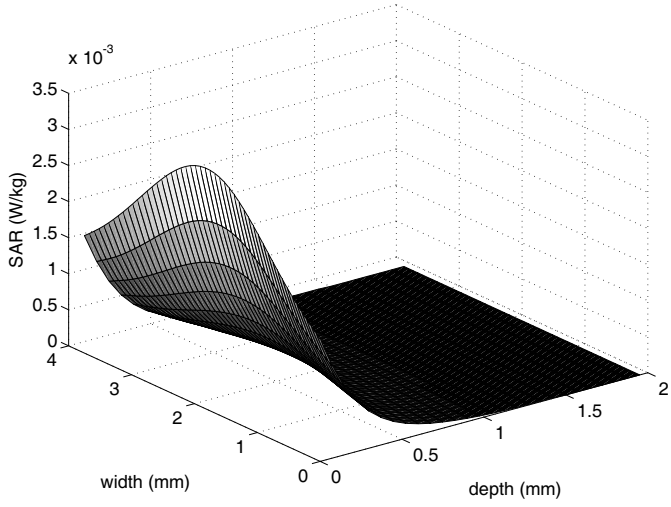

Figure 7. SAR of human skin at 61.22 GHz with respect to depth and width.

Furthermore, beyond 1.5 mm which is the fat layer, the human skin has negligible absorption at both frequencies. This is due to the fact that most of the electromagnetic energy has already been absorbed in the epidermis and dermis layers of the human skin, which results in

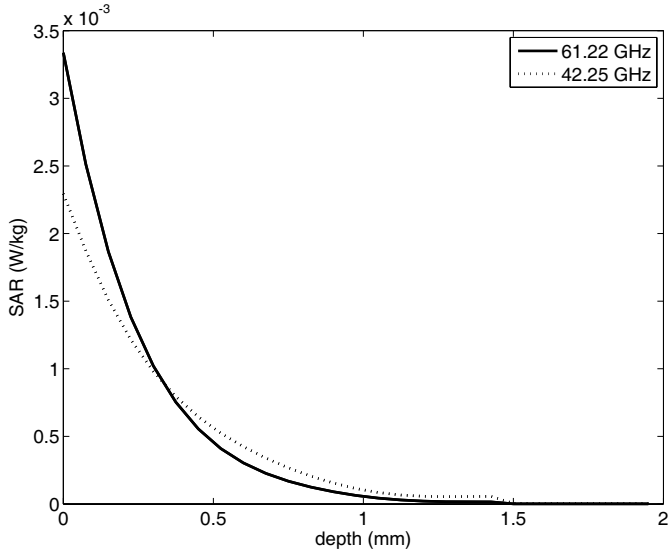

Figure 8. SAR of human skin at 42.25 GHz and 61.22 GHz with respect to depth.

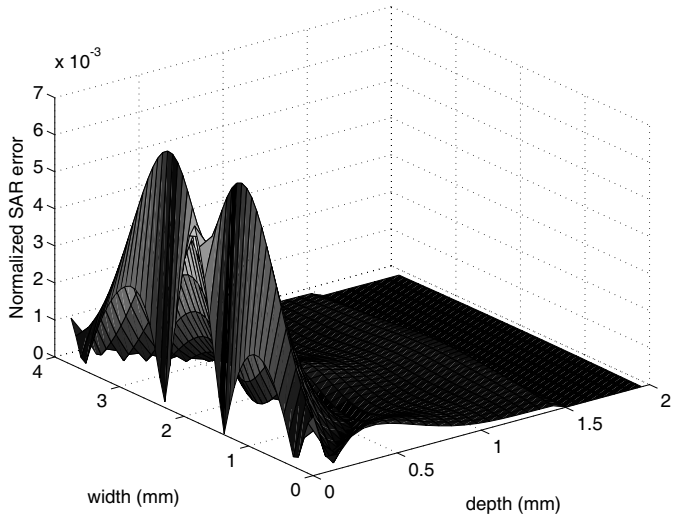

Figure 9. Normalized SAR error with respect to depth and width at 42.25 GHz for ETD scheme.

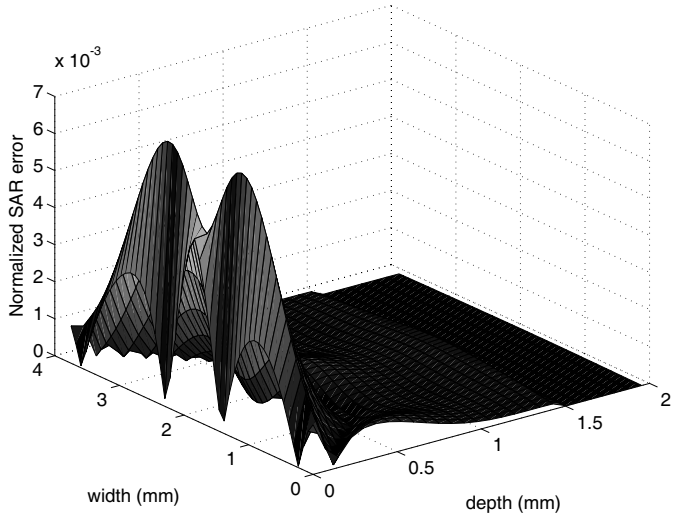

Figure 10. Normalized SAR error with respect to depth and width at 42.25 GHz for averaging scheme.

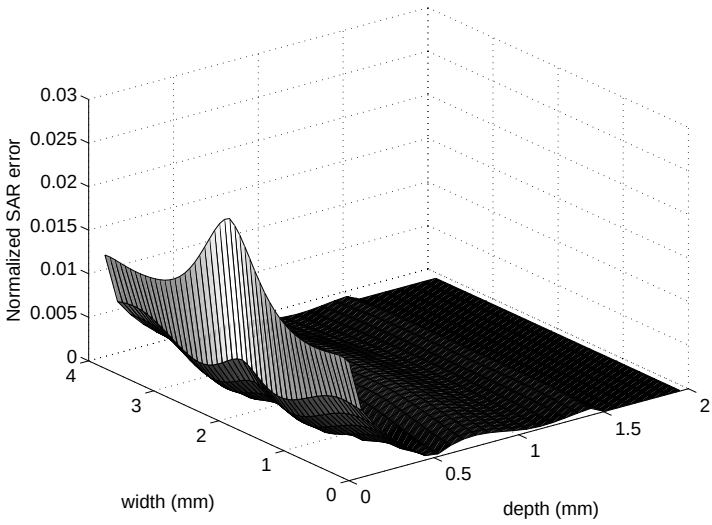

Figure 11. Normalized SAR error with respect to depth and width at 42.25 GHz for forward-forward scheme.

weak penetration of power into the fat layer.

For comparison, we have also computed the SAR using the efficient fundamental form of ADI-FDTD with averaging and forward-forward

schemes. As reference, the same numerical example is performed using the explicit FDTD method of time-averaging scheme [1]. The normalized SAR error is defined as

$$SAR_{error} = \frac{SAR_{ADI} - SAR_{explicit}}{\max(SAR_{explicit})} \tag{33}$$

where SAR_{ADI} is the SAR computed using various efficient fundamental form of ADI-FDTD schemes and $SAR_{explicit}$ is the SAR computed using the explicit FDTD method. Figs. 9, 10 and 11 show the normalized SAR error of ETD, averaging and forward-forward schemes at 42.25 GHz and z cut plane of 2 mm. It is seen that the forward-forward scheme incurs the highest error due to the fact that the scheme is only first-order in temporal accuracy. The ETD and averaging schemes are both second-order in temporal accuracy and thus, exhibits lower error.

6. CONCLUSION

This paper has presented the unified efficient fundamental ADI-FDTD schemes for lossy media. The schemes presented include averaging, forward-forward, forward-backward and novel exponential time differencing schemes. Unifications of these schemes in both conventional and efficient fundamental forms of source-incorporated ADI-FDTD have been provided. In the latter, they have been formulated in the simplest, most concise, most efficient, and most fundamental form of ADI-FDTD. The unified update equations and implementation of the efficient fundamental ADI-FDTD schemes have been provided. Such efficient fundamental schemes have substantially less RHS update coefficients and field variables compared to the conventional ADI-FDTD schemes. Thus, they feature higher efficiency with reduced memory indexing and arithmetic operations. Other aspects such as field and parameter memory arrays, PEC and PMC implementations have been discussed. Numerical results in the realm of CPU time saving, asymmetry and numerical errors as well as SAR of human skin have been presented.

REFERENCES

1. Taflove, F. and S. C. Hagness, *Computational Electrodynamics: The Finite-Difference Time-Domain Method*, Artech House, Boston, MA, 2005.
2. Namiki, T., "3-D ADI-FDTD method-unconditionally stable time-domain algorithm for solving full vector Maxwell's equa-

tions," *IEEE Trans. Microw. Theory Tech.*, Vol. 48, No. 10, 1743–1748, Oct. 2000.

3. Zheng, F., Z. Chen, and J. Zhang, "Toward the development of a three-dimensional unconditionally stable finite-difference time-domain method," *IEEE Trans. Microw. Theory Tech.*, Vol. 48, No. 9, 1550–1558, Sep. 2000.
4. Chen, C. C.-P., T.-W. Lee, N. Murugesan, and S. C. Hagness, "Generalized FDTD-ADI: An unconditionally stable full-wave Maxwell's equations solver for VLSI interconnect modeling," *IEEE/ACM Int. Conf. on Computer Aided Design*, 156–163, San Jose, CA, USA, Nov. 2000.
5. Garcia, S. G., T. W. Lee, and S. C. Hagness, "On the accuracy of the ADI-FDTD method," *IEEE Antennas Wireless Propagat. Lett.*, Vol. 1, No. 1, 31–34, 2002.
6. Fu, W. and E. L. Tan, "Stability and dispersion analysis for ADI-FDTD method in lossy media," *IEEE Trans. Antennas Propagat.*, Vol. 55, No. 4, 1095–1102, Apr. 2007.
7. Yuan, C. and Z. Chen, "Towards accurate time-domain simulation of highly conductive materials," *2002 IEEE MTT-S Int. Microwave Symp. Dig.*, 1135–1138, Seattle, WA, USA, Jun. 2002.
8. Pereda, J. A., A. Grande, O. Gonzalez, and A. Vegas, "The 1D ADI-FDTD method in lossy media," *IEEE Antennas Wireless Propagat. Lett.*, Vol. 7, 477–480, 2008.
9. Pereda, J. A., A. Grande, O. Gonzalez, and A. Vegas, "Analysis of two alternative ADI-FDTD formulations for transverse-electric waves in lossy materials," *IEEE Trans. Antennas Propagat.*, Vol. 57, No. 7, 2047–2054, Jul. 2009.
10. Heh, D. Y. and E. L. Tan "Lyapunov and matrix norm stability analysis of ADI-FDTD schemes for doubly lossy media," *IEEE Trans. Antennas Propagat.*, Vol. 59, No. 3, 979–986, Mar. 2011.
11. Tan, E. L., "Efficient algorithm for the unconditionally stable 3-D ADI-FDTD method," *IEEE Microw. Wireless Compon. Lett.*, Vol. 17, No. 1, 7–9, Jan. 2007.
12. Tan, E. L., "Fundamental schemes for efficient unconditionally stable implicit finite-difference time-domain methods," *IEEE Trans. Antennas Propagat.*, Vol. 56, No. 1, 170–177, Jan. 2008.
13. Heh, D. Y. and E. L. Tan, "Efficient implementation of 3-D ADI-FDTD method for lossy media," *2009 IEEE MTT-S Int. Microwave Symp. Dig.*, 313–316, Boston, Massachusetts, USA, Jun. 2009.
14. Holland, R., L. Simpson, and K. S. Kunz, "Finite-difference

analysis of EMP coupling to lossy dielectric structures," *IEEE Trans. Electromagn. Compat.*, Vol. 22, No. 3, 203–209, Aug. 1980.

15. Petropoulos, P. G., "Analysis of exponential time-differencing for FDTD in lossy dielectrics," *IEEE Trans. Antennas Propagat.*, Vol. 45, No. 6, 1054–1057, Jun. 1997.
16. Heh, D. Y. and E. L. Tan, "Dispersion analysis of FDTD schemes for doubly lossy media," *Progress In Electromagnetics Research B*, Vol. 17, 327–342, 2009.
17. Garcia, S. G., A. R. Bretones, R. G. Martin, and S. C. Hagness, "Accurate implementation of current sources in the ADI-FDTD scheme," *IEEE Antennas Wireless Propagat. Lett.*, Vol. 3, 141–144, 2004.
18. Donderici, B. and F. L. Teixeira "Symmetric source implementation for the ADI-FDTD method," *IEEE Trans. Antennas Propagat.*, Vol. 53, No. 4, 1562–1565, Apr. 2005.
19. Tan, E. L., "Concise current source implementation for efficient 3-D ADI-FDTD method," *IEEE Microw. Wireless Compon. Lett.*, Vol. 17, No. 11, 748–750, Nov. 2007.
20. Chen, J. and J. Wang, "PEC condition implementation for the ADI-FDTD method," *Microw. Opt. Technol. Lett.*, Vol. 49, No. 3, 526–530, 2007.
21. Rojavin, M. A. and M. C. Ziskin, "Medical application of millimeter waves," *Q. J. Med.*, Vol. 91, No. 1, 57–66, Jan. 1998.
22. Alekseev, S. I. and M. C. Ziskin, "Millimeter-wave absorption by cutaneous blood vessels: A computational study," *IEEE Trans. Biomed. Engineering*, Vol. 56, No. 10, 2380–2388, Oct. 2009.
23. Liu, S. and S. D. Gedney, "Perfectly matched layer media for an unconditionally stable three-dimensional ADI-FDTD method," *IEEE Microw. Guided Wave Lett.*, Vol. 10, 261–263, Jul. 2000.
24. Rubio, R. G., S. G. Garcia, A. R. Bretones, and R. G. Martin, "Crank-Nicolson reformulation of ADI-FDTD PML extensions," *IEEE Antennas Wireless Propagat. Lett.*, Vol. 5, No. 1, 357–360, 2006.
25. Tay, W. C. and E. L. Tan, "Split-field PML implementation for the efficient fundamental ADI-FDTD method," *2009 Asia Pacific Microw. Conf.*, 1553–1556, Singapore, Dec. 2009.
26. Tay, W. C., D. Y. Heh, and E. L. Tan, "GPU-accelerated fundamental ADI-FDTD with complex frequency shifted convolutional perfectly matched layer," *Progress In Electromagnetic Research M*, Vol. 14, 177–192, 2010.